

# Perceptual Coding for Compressed Video Understanding: A New Framework and Benchmark

Yuan Tian, Guo Lu, Yichao Yan, Guangtao Zhai, Li Chen, Zhiyong Gao

**Abstract**—Most video understanding methods are learned on high-quality videos. However, in most real-world scenarios, the videos are first compressed before the transportation and then decompressed for understanding. The decompressed videos are degraded in terms of perceptual quality, which may degenerate the downstream tasks. To address this issue, we propose the first coding framework for compressed video understanding, where another learnable perceptual bitstream is introduced and simultaneously transported with the video bitstream. With the sophisticatedly designed optimization target and network architectures, this new stream largely boosts the perceptual quality of the decoded videos yet with a small bit cost. Our framework can enjoy the best of both two worlds, (1) highly efficient content-coding of industrial video codec and (2) flexible perceptual-coding of neural networks (NNs). Finally, we build a rigorous benchmark for compressed video understanding over four different compression levels, six large-scale datasets, and two popular tasks. The proposed Dual-bitstream Perceptual Video Coding framework Dual-PVC consistently demonstrates significantly stronger performances than the baseline codec under the same bitrate level.

**Index Terms**—Video understanding, video compression, video restoration, contrastive learning.

## 1 INTRODUCTION

VIDEO understanding tasks, *e.g.*, action recognition and spatial-temporal action detection, have drawn more and more attention in the computer vision research community over the past few years. Although impressive performances have been achieved by exploiting deep neural networks (NNs) [1] [2] [3] [4] [5] [6] and large-scale video datasets [7] [8] [9] [10] [11], these tasks still face various challenges in the real-world scenarios, such as unstable illumination, camera lens aging and compression artifacts, just to name a few. We focus on the last challenge in this paper, since the video compression module is widely equipped with almost every video understanding (or surveillance) system to save the transportation cost or storage space.

Although video compression has a strong impact on the final video understanding performance, few works [12] [13] have discussed the problem. In fact, most previous video understanding methods are only evaluated with moderately compressed videos, where the video is almost the same as the original one. However, in many real-world scenarios, video understanding is usually a downstream task of the video compression, forming an *video transportation plus understanding* system. Therefore, it is highly demanded to investigate the system-level trade-off between the transportation bitrate and the video understanding performance.

Recently, Yochai *et al.* [14] extended the traditional rate-distortion theory [15] to the triplet rate-distortion-perception trade-off theory. Given a target bitrate constraint, they proved that the tradeoff of a compression system between *perception* and *distortion* is monotone and convex for any distortion measure

- Yuan Tian, Yichao Yan, Guangtao Zhai, Li Chen, and Zhiyong Gao are with Shanghai Jiao Tong University, China. Corresponding authors: Yichao Yan and Guangtao Zhai. E-mail: {ee\_tianyuan, yanyichao, zhaiguangtao, hilichen, zhiyong.gao}@sjtu.edu.cn.
- Guo Lu is with Beijing Institute of Technology, China. E-mail: guo.lu@bit.edu.cn.

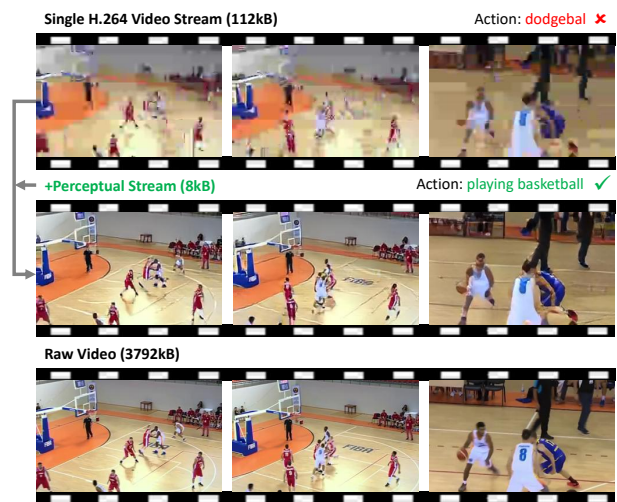


Fig. 1: Key objects such as basketball hoop are severely corrupted within the video decoded from H.264 stream, inducing the degenerated recognition result. By introducing a small *perceptual stream* (only 8kB), our framework decodes out the perceptually good video that can be easily recognized by the same action recognition model (TSM [4]). The video is from Kinetics [9]. *Best to view by zooming-in.*

such as PSNR and SSIM [16]. Therefore, when the transportation bitrate is heavily constrained in real-world applications, the video codecs oriented to better distortion quality cannot guarantee good perceptual results. This may degrade the performance of downstream video understanding tasks. Therefore, there arises an urgent issue that can we improve the perceptual coding performance of the current codecs.

To address this issue, we propose to transport another perceptual stream along with the original video stream by codecs. As shown in Fig. 1, the video decoded from the video stream preserves most texture elements, but it loses high-level information such as object edges and global contour, which is important for

human perception. When simultaneously transporting this information in the perceptual stream, our framework produces videos close to the raw video in terms of perceptual quality. Besides, the bit cost of the perceptual stream is small, due to the sparsity of the high-level information. We name this framework Dual-bitstream Perceptual Video Coding framework (Dual-PVC), as it includes two bitstreams. To constrain the overall bitrate of Dual-PVC while ensuring the high perceptual quality of the decoded frames, we optimize the framework end-to-end targeting a rate-perception trade-off. However, there are two obstacles that hinder the optimization procedure. **First**, although it is trivial to estimate the rate item [17], the optimization target for video perception is hard to determine. Few works study the video perception metric with the video transportation budget in mind. **Second**, the introduced perceptual stream should be complementary to video stream, so that the overall bit cost of the framework is small.

To optimize the video perceptual quality, we introduce an edge map-based perceptual loss, where a learnable edge map is used to measure the perceptual similarity between two videos. The motivations of adopting the edge representation to measure the perceptual quality are two folds. First, the edge map has been widely employed to guide the restoration of human-perceptive artifacts in many previous works on video compression [18] [19] [20] and image inpainting [21]. Second, the edge map is binarized and discards most of the textures in the original frame. Therefore, preserving the edge information requires small extra bit costs, which is beneficial for building a transportation-efficient video understanding system. Particularly, the edge map is jointly learned with other components following a contrastive learning manner with unlabeled video data during training.

To make the introduced perceptual stream complementary to the video codec stream, its encoder follows a two-pathway paradigm, which includes an encoder pathway and a difference map pathway. The difference map denotes the difference between the compressed video by the codec and the original one, which indicates the information lost during the video coding procedure. Under the guidance of this difference signal, the encoder can mostly encode the information that is omitted by the video codec. Furthermore, we dynamically generate the region-adaptive convolution kernels that are specified for the omitted regions. Each kernel is adaptively aggregated from a kernel pool, which is also adaptive to the context of the current video. The video features extracted by the above highly-dynamic kernels are finally encoded by entropy encoders such as arithmetic coding [22], and constitute the perceptual stream.

Although most (if not all) video understanding tasks can be integrated into our framework, we take the action recognition and spatial-temporal action detection tasks as examples to evaluate our framework. We validate our proposed framework under four different bitrate levels on six large-scale video datasets: (1) action recognition task with five datasets, *i.e.*, Kinetics-400, Something-to-Something, UCF101, HMDB51, Diving48 and (2) spatial-temporal action detection task with the large-scale AVA dataset. The evaluations are conducted upon several popular downstream task models, *i.e.*, TSM [4], SlowFast networks [3] and TimeSformer [23]. Our framework demonstrates strong performance on all datasets and models. Moreover, since all components of our framework are differentiable, we can further improve it by jointly training it with the specified downstream model.

To summarize, our main contributions are:

- To the best of our knowledge, this work is the first to

address the degradation of video understanding tasks caused by video compression. To facilitate future research, we build a systematical benchmark by evaluating five downstream models on six large-scale video datasets under four different compression levels.

- We propose the Dual-bitstream Perceptual Video Coding framework (Dual-PVC), which introduces a novel perceptual stream beyond the traditional single video stream scheme. Dual-PVC significantly improves the downstream video understanding task performance at the same bitrate budget.
- An edge map-based perceptual loss is proposed to optimize the quality of the videos decoded from the framework. Particularly, the edge map representation is learned from the raw video data in a self-supervised manner.
- To ensure the compression efficiency of the perceptual stream, a two-pathway dynamic encoder is proposed to enforce the stream mostly encoding the information omitted by the video stream.
- The proposed Dual-PVC framework is trained once and deployed for every downstream task/model, yet demonstrating strong performances on all evaluated tasks and datasets. Moreover, its performance can be further improved by being fine-tuned on a specific task/model.

## 2 RELATED WORKS

### 2.1 Action Recognition on Compressed Videos

Recently, some works have been proposed to perform action recognition on compressed videos. They mainly differ from the standard video recognition methods in terms of the input modality. Instead of the raw RGB frames decoded from the compressed video stream, these works directly take in the extracted intra-prediction frame (I-frame), motion vector and residual frame as the input. In the pioneering work [24], they replace the computationally extensive optical flow input modality used in the traditional two-stream network with the off-the-shelf motion vector decoded from the MPEG stream. Latter, following up works achieve better performance by further exploiting the residual frames [25] or refining motion vectors with the supervision of pre-calculated optical flow [26]. Recently, MVCGC [27] leverages the decoded RGB frames and motion vectors as the positive pair to perform contrastive learning, aiming to learn a robust video representation that can be transferred to the downstream tasks.

We highlight that our defined problem is fundamentally different from them. First, these works avoid discussing the trade-off between the transportation bit rate and the downstream task performance, which is one of the most important aspects of a “video transportation plus downstream tasks” system. Second, the video stream leveraged by these works is extracted from the original video files of the released datasets, which are recorded in high bitrates. This cannot satisfy the practical applications, since we expect stable performance across various bitrates.

Very recently, Yi *et al.* [12] evaluated the robustness of several video action recognition models to several common corruptions, which include the compression artifacts. However, they just reveal the intuitive conclusion that video compression degrades the action recognition performance severely. In contrast, we propose a new framework to systematically address this issue.

## 2.2 Deep Video Understanding

**Action recognition:** Most prior methods focus on modeling the high-level spatial-temporal information from the videos by employing temporal fusion operations or 3D CNNs. For example, two-stream CNNs [28] [29] leverage the RGB input and the optical flow input in two separate pathways, achieving much better performance than a single RGB stream paradigm. Due to the inefficiency of the optical flow modality, the latter works mainly model the motion cues in feature space. For example, the temporal segment network (TSN) [30] adopts a simple averaging function to aggregate features of each frame. The subsequent works (TRN [31], TSM [4], TEA [5], TEINet [32], TDN [33], TAM [34] ) improves TSN by introducing more sophisticated temporal modeling modules. To simultaneously learn the temporal evolution along with the spatial information, 3D networks, *e.g.*, C3D network [1] [35], I3D [9], 3D-ResNet [36] [37], R(2+1)D CNNs [38] [39], Slowfast networks [3], and X3D networks [40] are continuously proposed. I3D [9] proposes to inflate the 2D CNNs [41] [42] pre-trained on ImageNet [43] by copying weights. Slowfast networks [3] involve a slow pathway to capture spatial semantics at low frame rate and a fast pathway to capture motion at fine temporal resolution. Very recently, Gedas *et al.* [23] proposed the first pure-Transformer architecture for video understanding, which involves several self-attention designs over space-time dimensions.

**Action detection:** Most methods [44] [3] [45] [46] [47] follow a two-stage pipeline, which has been extensively verified in the object detection field. In the first stage, they take the keyframe of a video clip as the input to an object detection model, obtaining the bounding box of actors. Then, they feed the video clip and the actor bounding boxes to the 3D video backbone network to extract features in the region of interest (RoI) for predicting the action class. Recently, there are few methods [48] simplifying the pipeline into one stage.

In this paper, we establish the benchmark of compressed video understanding by performing extensive experiments on several 2D/3D/Transformer-based models of the two popular tasks above.

## 2.3 Video Restoration

Our framework can be also categorized into the generalized “video restoration followed by video understanding” scheme. Therefore, we also give an overview of the video restoration topic. Xue *et al.* [49] designed a neural network with a motion estimation and a video processing component, and utilized a joint training strategy to handle various low-level vision tasks. Lu *et al.* [50] further incorporated a quantized prediction residual in compressed code streams as strong prior knowledge, and proposed a deep Kalman filter network (DKFN) to utilize the spatio-temporal information from the preceding frames of the target frame. In addition, considering the quality of nearby compressed frames dramatically fluctuates, Yang *et al.* [51] proposed a multi-frame quality enhancement (MFQE) module and utilized motion compensation of two nearest PQFs to enhance low-quality frames. Without explicit motion compensations, Jo *et al.* [52] utilized a 3D convolutional network as a dynamic filter generation network to generate a dynamic upsampling filter and fine residual details. More recently, STDF [53] leverages the deformable convolution [54] to learn a more flexible motion compensation.

However, all these methods are blind (*a.k.a.*, unconditioned) and optimized with one specific compression level, thus struggling

on restoring various in-the-wild compression artifacts. Moreover, these methods are ineffective on large distortions caused by high compression levels, which are common in real-world network bandwidth-constrained scenarios. In contrast, we simultaneously address both the above two problems by using another perceptual stream as the condition of the restoration procedure.

## 2.4 Video Compression

Our work is also closely related to the video compression topic. For the traditional video codecs [55] [56], different linear transformations are exploited to better capture the statistical characteristics of the texture and motion information within the videos. For example, The basic transform adopted in H.264 codec [55] is a scaled approximate Discrete Cosine Transform (DCT) with fixed block sizes. H.265 codec [56] uses integer DCT and DST transforms with varied block sizes. Latter, learnable video codecs [57] [58] [59] [60] [61] [62] [63] gain increasing attention. Following the traditional hybrid video compression framework, Lu *et al.* [57] proposed the first end-to-end optimized video compression framework, in which all the key components in H.264/H.265 are replaced with deep neural networks. Latter, Lin *et al.* [58] exploited multiple frames in different modules to further remove the redundancy. Hu *et al.* [59] proposed a resolution-adaptive optical flow compression method.

Recently, Yang *et al.* [64] proposed a recurrent conditional GAN for learnable perceptual video compression. However, this work aims to generate videos of good visual quality, in terms of qualitative or quantitative metrics. In contrast, our framework mainly focuses on building a perceptual video coding framework that is beneficial to the downstream video understanding tasks.

## 3 APPROACH

We propose a dual-bitstream perceptual video coding framework Dual-PVC for compressed video understanding tasks, as shown in Fig. 2. We first give a brief introduction to the framework.

**Video Stream:** Given a high-quality (HQ) video  $X$  captured by edge devices, it is compressed to a video stream by a video codec such as the H.264 codec before being transported, and will be decoded as the video  $\tilde{X}$  when received on the cloud side. In most cases,  $\tilde{X}$  is of low quality and contains compression artifacts, due to the information lost during the compression procedure.

**Perceptual Stream:** As we have discussed in section 1, directly restoring the video from  $\tilde{X}$  may not achieve perceptually-good results. Hence, we introduce the perceptual stream  $\mathcal{S}$  to assist the restoration procedure, which is produced by a learnable NN-based encoder Enc-Net. Particularly, Enc-Net makes full use of the RGB difference map  $D$  before/after video codec as the guidance signal, facilitating itself to mainly encode the information that is lost by video stream. Both the video and perceptual streams are encoded on the edge (*a.k.a.*, sender) side.

**Cloud Side:** After the two streams are transported and received on the cloud (*a.k.a.* recipient) side, a video restoration network (R-Net) is employed to restore the perceptually-good video  $\hat{X} := \text{R-Net}(\tilde{X}, \mathcal{S})$ . Finally,  $\hat{X}$  is fed into various downstream task models.

Next, we elaborate on the components above in detail.

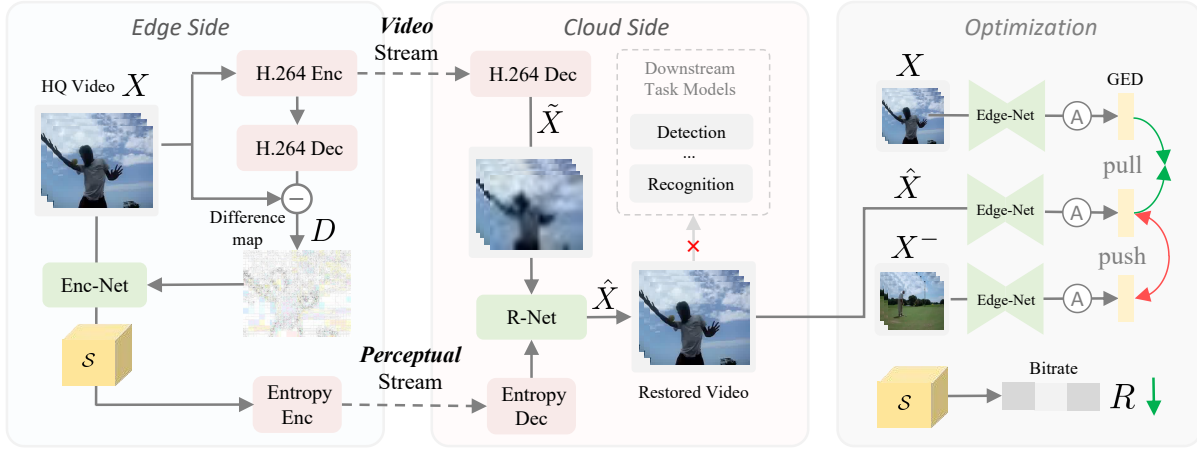


Fig. 2: **Dual-PVC Framework** includes two bitstreams. The one is the *video* stream produced by video codecs. Another stream is the *perceptual* stream, which encodes video perceptual information that is lost by the previous one. The perceptual stream  $\mathcal{S}$  is produced by a learnable encoder (Enc-Net) deployed on the edge side. On the cloud side, the raw decoded video  $\tilde{X}$  is first restored as  $\hat{X}$  by R-Net with the guidance of  $\mathcal{S}$ . Then,  $\hat{X}$  is fed into the downstream task models.  $\times$  denotes the downstream models are detached during the training. The whole framework is optimized by pushing an edge map-based perceptual descriptor GED of the  $\hat{X}$  closer to that of the original video  $X$ . Edge-Net represents a shallow network for extracting the edge map and “A” denotes aggregating the maps into a video-level representation.

### 3.1 Perceptual Stream Encoder (Enc-Net)

We consider two requirements of the Enc-Net deployed on the edge device. (1) The produced structure stream should be complementary to the video stream. (2) Enc-Net should be proficient in extracting expressive feature representation for various objects in videos. To fit the first requirement, we propose to exploit the compression difference map  $D := X - X_{lb}$  by video codecs to guide the perceptual encoding procedure. The difference map enforces the Enc-Net to mainly encode the information omitted by the video codec. Note that calculating  $D$  on the edge side is feasible by performing an extra video decoding operation, which adds a little computational burden. To meet the second one, we propose to dynamically generate convolution kernels that are specific for each region of the video frame. In this way, the representation capability can be largely enhanced since different objects can be concurrently represented by a single channel. Besides, this design is also friendly to computational cost and memory consumption. The smaller channel number, the more resources can be saved.

**Overall architecture.** As shown in Fig. 3 (a), Enc-Net follows a two-pathway architecture. One is the feature encoding pathway taking the video frame  $X^i$  as input, and the other is the difference map stream. Both the two pathways include five stages, each of which includes a downsampling CNN denoted as Down with downscaling ratio two in terms of spatial scale. After each block, the features output from the two pathways are fused by a lateral connection module, *i.e.*, difference guided fusion module (D-GFM). These steps can be formulated as:

$$\begin{aligned} x_{l+1}, d_{l+1} &= \text{D-GFM}(\text{Down}(x_l), \text{Down}(d_l)), \\ x_0 &= X^i, d_0 = D^i, \end{aligned} \quad (1)$$

where  $i$  indicates the frame index, the parameters of Down are not shared across the two pathways. The frame features  $x_4$  output from the last stage (the 4th stage) are further processed by a light-weight 3D CNN to remove the inter-frame redundancy between the consecutive frames, producing the video-level perceptual feature  $\mathcal{S}$ . Here, the 3D CNN consists of two stacking 3D convolutions with spatial-temporal kernel size 5 and group number 32.  $\mathcal{S}$  is then encoded to the bitstream by an entropy encoder.

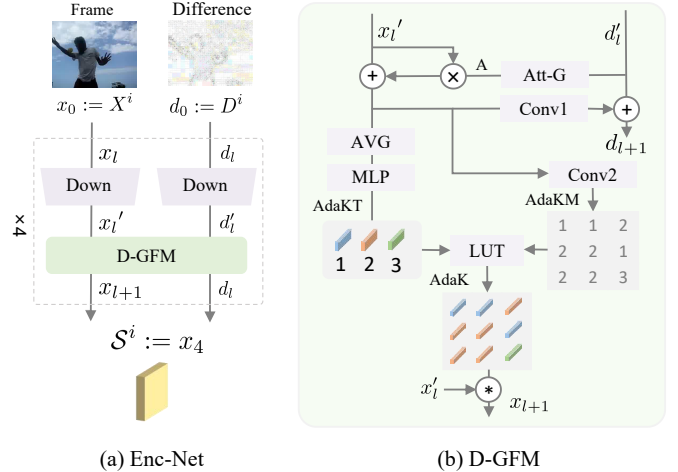


Fig. 3: Perceptual stream encoder (Enc-Net) hierarchically downsamples the video frame  $X^i$  and the compression difference map  $D_i$ , producing the perceptual feature  $\mathcal{S}^i$ . The intermediate features from the two pathways are fused by the difference guided fusion module (D-GFM), where the adaptive kernel (AdaK) are assembled from the adaptive kernel table (AdaKT) and the region-adaptive kernel index map (AdaKM) via a look-up-table (LUT) operation.

**D-GFM:** D-GFM is introduced to fuse the features in two pathways, enabling them cooperate with each other. More importantly, it exploits the difference map features  $d_l$  to adaptively strengthen the encoding of the low-quality regions, so that highly-efficient compression can be achieved given the limited bit cost constraint. As shown in Fig. 3 (b), the fusion procedure consists of three sub-steps:

(1) **Frame feature enhancement.** Concretely, given the frame feature  $x'_l := \text{Down}(x_l)$ ,  $x'_l \in \mathbb{R}^{C \times H \times W}$  and the artifact feature  $d'_l = \text{Down}(d_l)$  output from the downsampling CNN, we adopt  $d'_l$  to produce the attention map  $A \in \mathbb{R}^{C \times H \times W}$ , which is used to selectively enhance  $x'_l$ , producing  $\tilde{x}_l$ :

$$\tilde{x}_l = x_l + A \cdot x_l, A = \text{Sigmoid}(\text{Att-G}(d_l)), \quad (2)$$

where Att-G is implemented as two stacked group convolution of kernel size  $3 \times 3$ ,  $\cdot$  denotes the element-wise multiplication.

(2) **Adaptive kernel table (AdaKT) generation.** Then, we leverage the global statistics of  $\tilde{x}_l$  to estimate an adaptive kernel table  $\text{AdaKT} \in \mathbb{R}^{N \cdot C \cdot 5 \cdot 5}$ , which consists of  $N$  depth-wise convolution kernels of size  $5 \times 5$ .  $\text{AdaKT} := \text{MLP}(\text{AVG}(\tilde{x}_l))$ , where MLP denotes a three-layer multi-layer perceptron with ReLU non-linearity [65]. AVG denotes the spatial average pooling, which captures the global statistics of each frame. Although more sophisticated architectures can be used to adaptively produce the convolution kernel for each frame, we find this SE-style architecture [66] works well and is efficient. Compared to the shared static convolution kernels in plain CNN architectures, the convolutional kernels within AdaKT are specified for the objects in the current frame  $X^i$ . We adopt larger convolution kernel size, *i.e.*,  $5 \times 5$ , so that more spatial redundancies can be detected and compressed in the following steps, which is the common practice in works [67] [68] [57] on image/video compression.

(3) **Region-adaptive feature extraction.** To allocate the kernels within AdaKT to the appropriated regions, we further adopt a  $3 \times 3$  convolution denoted as Conv2 to dynamically generate a region-adaptive kernel index map (AdaKM) by comprehensively considering the frame feature and the compression difference information:  $\text{AdaKM} = \text{Conv2}(\tilde{x}_l \circ d_l)$ , where  $\circ$  denotes the channel-wise concatenation operation.  $\text{AdaKM} \in \mathbb{R}^{N \cdot C \cdot 5 \cdot 5}$  is immediately inflated into a spatial-adaptive kernel  $\text{AdaK} \in \mathbb{R}^{C \times W \times H \times 5 \times 5}$  by replacing each index with the kernel from AdaKT using look-up-table (LUT) operation. Given AdaK, the frame feature  $x_{l+1}$  is extracted by the depth-wise pixel-adaptive convolution operation [69], and then fed to the next stage. The LUT operation can be approximated by a differential soft-argmax operation during training. Besides, the difference feature is also modulated by the enhanced frame feature,  $d_{l+1} = d_l + \text{Conv1}(\tilde{x}_l)$ , aiming to provide more precise guidance information for the next stage. Conv1 is a two-layer convolution network with kernel size one.

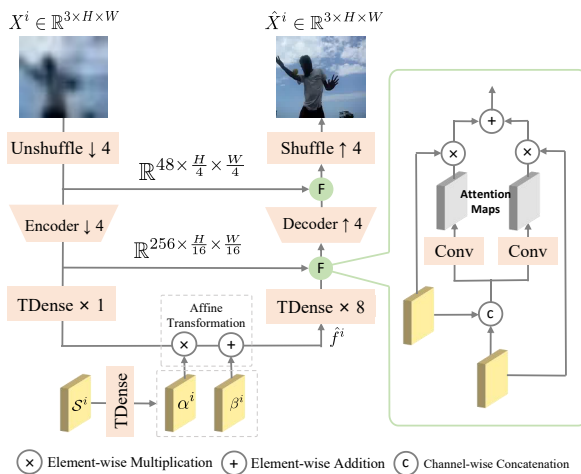


Fig. 4: Video restoration network (R-Net).  $\downarrow 4$  and  $\uparrow 4$  denote downscaling and upscaling the input by 4 times. TDense represents the temporal modeling enhanced dense block. We also introduce an attention-based fusion module for adaptively fusing the information in the downscaling and the upscaling procedures, which is illustrated in the right part.

### 3.2 Video Restoration Network (R-Net)

Most of the previous video restoration methods [49] [50] [51] [50] [52] are blind to specific distortion types, and rely on very large neural networks to estimate the distribution of the unknown artifacts. To achieve a more accurate estimation for each pixel, these works usually follow the “motion compensation plus refinement” paradigm to exploit the temporal information, where motion is usually represented as the computationally expensive dense optical flow.

Instead of restoring the pixel-level details, we mainly aim to complete the video structure distortion, which is more sensitive to human perception. Therefore, we perform the procedure in the *low-resolution* space, employing a simple UNet-style [70] restoration network equipped with extra temporal convolutions to process the video frames, as shown in Fig. 4. Specifically, a pixel shuffle operator first losslessly downscales the input video frame  $X^i$  by a factor of four. To further reduce the spatial resolution and strengthen the non-linearity of the transformation, we leverage an encoder CNN to further downscale the feature by a factor of four while increasing the channel number, where the encoder consists of two LeakyReLU [71] activated convolution with stride size 2. The features are further processed by four consequential temporal modeling enhanced dense blocks (TDense), producing the ultimate feature  $f_i$ . In this deep latent space, we make full use of the received perceptual information  $\mathcal{S}$ . Typically, we adopt the affine transformation to fuse the information in  $\mathcal{S}$  and  $f_i$ , producing  $\hat{f}^i = f_i \cdot \alpha^i + \beta^i$ , where  $\alpha^i$  and  $\beta^i$  are the first and second half parts of the tensor transformed from  $\mathcal{S}$  by a TDense block, *i.e.*,  $\alpha^i \circ \beta^i = \text{TDense}(\mathcal{S})$ . Then, the  $\hat{f}^i$  is decoded into the restored video frame  $\hat{X}^i$  by the inverse encoding procedure. Besides, skip connection designing is also incorporated to reuse low-level features and prevent gradient vanishing.

**Up-Down Path Fusion.** Instead of the simple channel-wise concatenation fusion scheme used in the original U-Net, we introduce the attention mechanism to adaptively preserve the information beneficial to human perception. The motivation is that the features may contain the compression artifact information, and should be masked by an attention map. The attention maps are produced by a group convolution of group size 8 and kernel size 3 followed by a pointwise convolution [72], which is denoted as Conv in Fig. 4.

**TDense.** The TDense block is modified from the vanilla Dense2D block [73] by replacing the last standard spatial convolution layer with the multi-scale temporal convolutions. Specifically, the first and the second half number channels are fed into the temporal convolutions of kernel sizes three and five, respectively. This simple improvement not only enhances the Dense2D block with the temporal modeling capability that is critical for processing video data, but also reduces the computational cost.

### 3.3 Contrastive Learning of Video Perceptual Metric

The most straightforward learning target for the proposed Dual-PVC framework is to minimize the task prediction error of the restored video  $\hat{X}$ , where the supervisory signal is the ground-truth label or the pseudo label generated by the downstream models. However, there are several issues that hinder the practical employment of this scheme. **First**, jointly training all downstream tasks/models with the proposed framework may be infeasible, considering that the training cost of the downstream video models is prohibitive. For example, training a SlowFast [3] model on

Kinetics with eight GPUs usually takes more than three days. **Second**, the downstream model and the training data may be inaccessible due to safety or privacy concerns, which is common in industrial scenarios.

**Learning of Edge Map.** To address these issues, we propose a (downstream) model-agnostic video perceptual metric, which is calculated by a learnable distance function  $\mathcal{D}$  defined in the low-dimensional feature representation space. This video-level representation termed global edge descriptor (GED) is aggregated from the frame-level edge maps. To discriminate the global structures of different videos, a loose constraint for GED is only required, *i.e.*, the distance between the restored video and the original high-quality video is much smaller than the distance between the decoded video and any other high-quality video instances:

$$\mathcal{D}(\text{GED}(\hat{X}), \text{GED}(X)) \ll \mathcal{D}(\text{GED}(\hat{X}), \text{GED}(X^-)), \quad (3)$$

where the negative video sample  $X^-$  is randomly sampled from the video dataset. In fact, the structure descriptor  $\text{GED}$  and the distance function  $\mathcal{D}$  can be simultaneously learned from the unlabeled video data following a contrastive learning manner:

$$\mathcal{L}_{con} = \log \frac{\exp(\mathcal{D}(\text{GED}(\hat{X}), \text{GED}(X))/\tau)}{\sum_{i=1}^B \exp(\mathcal{D}(\text{GED}(\hat{X}), \text{GED}(X_i^-))/\tau)}, \quad (4)$$

$$\mathcal{D}(x, y) = \cos(\phi \cdot a, \phi \cdot b),$$

where  $\phi$  denotes a two-layer MLP head with hidden number 512,  $B$  denotes the number of samples in the minibatch,  $\cos$  denotes the cosine similarity, and  $\tau$  is a temperature hyper-parameter adjusting the scale of cosine similarities.

**Global Edge Descriptor (GED).** We propose to aggregate the edge map of each video frame to form the global perceptual descriptor of the video. Specifically, Given one frame  $X_i$  of the video  $X$ , a lightweight CNN Edge-Net is utilized to extract the edge map of it:

$$M_i = \text{Edge-Net}(X_i), M_i \in \mathbb{R}^{1 \times H \times W}, \quad (5)$$

where the encoder part of Edge-Net is implemented as two stacking residual blocks with downsampling ratio four, and the architecture of the decoder part is symmetrical to the encoder. The tail of the Edge-Net is a Sigmoid activation function so that the produced edge maps are normalized.

Then, we adopt a two-layer MLP to compress each  $16 \times 16$  patch of  $M_i$  as a 128-dimensional vector. These vectors form a feature map of size  $\mathbb{R}^{128 \times \frac{H}{16} \times \frac{W}{16}}$ . Taking inspiration from the positional encoding technique in Transformers [74], we introduce a positional token  $Pos \in \mathbb{R}^{128 \times \frac{H}{16} \times \frac{W}{16}}$  of the same size and add it to the above feature map.  $Pos$  explicitly allocates a learnable descriptor for each position. Then, a residual block followed by an average pooling operation produces the frame-level edge descriptor. Finally, The frame-level edge descriptors of a video are aggregated as a video-level descriptor  $\text{GED}(X)$  by a lightweight temporal convolution network [75].

**Edge Map-Based Perceptual Loss.** Although  $\mathcal{L}_{con}$  jointly optimizes Edge-Net and the global video perceptual metric, the local structures are not constrained, which are also critical for the video perceptual quality. Therefore, we also regularize the pixel-wise edge map consistency between the original video and the decoded video:

$$\mathcal{L}_{local} = \|\text{Edge-Net}(\hat{X}) - \text{Edge-Net}(X)\|_2. \quad (6)$$

Finally, the edge map-based perceptual loss is given by:

$$\mathcal{L}_{edge} = \mathcal{L}_{con} + \mathcal{L}_{local}. \quad (7)$$

### 3.4 Optimization of Framework

The target of the proposed Dual-PVC framework is to maximize the perceptual quality of the restored video  $\hat{X}$ , while in the meanwhile minimizing the number of bits used for the introduced perceptual stream. We also regularize the domain gap between the restored video  $\hat{X}$  and the original video by the GAN loss, ensuring that  $\hat{X}$  is readily fed into the various downstream video understanding modules without jointly training.

$$\mathcal{L} = \underbrace{\alpha \mathcal{L}_{edge} + \mathcal{L}_{l_{pips}}}_{\text{perceptual}} + \lambda \underbrace{H(S)}_{\text{bitrate}} + \underbrace{\mathcal{L}_{GAN}}_{\text{domain}}, \quad (8)$$

where  $\lambda$  is used to control the target bitrate of the perceptual stream,  $\alpha$  is the balancing weight for  $\mathcal{L}_{edge}$ . Previous works on learnable video/image compression usually set  $\lambda$  to a small value such as  $\frac{1}{256}$ . Different from them, we set it to a much larger value, *i.e.*,  $\lambda = 1$ , so that the bitrate of the perceptual stream is constrained to be small.

**Perceptual metric.** We adopt two perceptual metrics as the loss function to regularize the restored video  $\hat{X}$  is perceptually-good and friendly to the downstream video understanding tasks. The first one is the proposed  $\mathcal{L}_{edge}$ . However, since the patch-wise texture distribution can not be regularized by  $\mathcal{L}_{edge}$ , the restored video will easily fall into an unpredictable and stochastic color space, which has also been recently observed in [76]. Therefore, we also introduce the learned image perceptual loss [77]  $\mathcal{L}_{l_{pips}}$  to hierarchically regularize the patch-wise distribution. We adopt the feature maps from the VGG16 network [78] pre-trained on ImageNet [43] to calculate  $\mathcal{L}_{l_{pips}}$ .

**Bitrate estimation.** The perceptual feature  $S$  will be quantized and transformed into the bitstream for transmission by performing entropy coding. During the training procedure, a differentiable quantization operation is required before the coding procedure. Following [67], we approximate the quantization operation by adding the uniform noise in the training stage. In the inference stage, we directly use the rounding operation. For the estimation of bitrate  $H(S)$ , we employ the basic entropy model in [68], although more advanced entropy models such as hyper-prior model and auto-regressive models can also be adopted in our framework.

**Details of GAN.** The discriminator is the same as the Patch-GAN [79], and hinge adversarial loss [80] is adopted.

## 4 EXPERIMENTS

### 4.1 Video Datasets

For *action recognition* task, we evaluate it on 5 large-scale video datasets, UCF101 [8], HMDB [7], Kinetics [9], Something V1 [10], and Diving48 [11]. The first three datasets focus on appearance-based actions such as “playing basketball”, while the actions in the last two datasets rely on temporal reasoning. For *spatial-temporal action detection* task, we adopt the widely used large-scale AVA dataset [81].

**UCF101 & HMDB.** The UCF101 [8] and HMDB51 [7] datasets contains 13,320 and 6,766 video clips. We adopt the first split of the official training/testing protocols for evaluation.

**Kinetics.** Kinetics [9] is a large-scale challenging human action recognition dataset, including more than 200k training

videos. We evaluate our models on the Kinetics-400 to prove that our framework is also applicable to very large-scale video datasets.

**SomethingV1 & Diving48.** SomethingV1 dataset [10] contains about 110k videos covering 174 fine-grained action categories with diverse objects and scenes. Diving48 [11] is a newly released dataset with more than 18K video clips for 48 unambiguous diving classes. Since the recognition of these actions require temporal seasoning, we conduct experiments on this dataset to verify the video dynamics modeling capability of our framework.

**AVA.** The AVA dataset [81] is one recent representative benchmark dataset for testing the spatio-temporal action localization performance. It contains about 211k training clips and 57k validating video clips. Following the standard protocol adopted by previous works [3] [82], we evaluate 60 classes among total 80 classes. The evaluation of the whole dataset is very time-consuming, especially when introducing the online video coding pipeline. Therefore, we randomly sample five videos from the original 430 video clips, resulting 4102 clips as the validation set. The subset is named AVA2.1 $^\diamond$ . The sampled video file names are *5BDj0ow5hnA*, *6d5u6FHvz7Q*, *9Y\_19NsnYEO*, *BXCh3r-pPAM* and *CMCPhm2LA00*.

## 4.2 Evaluation Settings

**Blind.** In this setting, both the downstream tasks and models are unknown. We use the unlabeled videos to optimize the framework, then we directly test it on different downstream tasks and models. This setting is friendly to the practical deployment, *i.e.*, the deployed framework can integrate the current downstream task modules seamlessly, no matter the modules are differentiable/accessible or not. For example, the module is ensembled by several models thus indifferentiable, or the downstream video understanding module is provided in the form of an online Application Programming Interface (API) service.

**Customized.** In this setting, the framework is customized to the downstream differential models. The models are accessible but may be prohibitive to be changed, due to the safety concern. We fine-tune the framework based on the model pre-trained on the blind setting.

## 4.3 Baseline Downstream Models

For the *action recognition* task, we adopt the following popular models as our baselines, *i.e.*, TSM [4], SlowFast networks [3], and TimeSformer [23], including 2D CNN, 3D CNN and the recent Transformer architectures. Both the pre-trained models and the sampling strategies are adopted from the MMAction2 framework [83], except that we always use the simple-clip&center-crop setting during evaluation. The reason is that the “testing augmentation+online compression” scheme costs in-affordable evaluation time. For the *action detection* task, we adopt the FasterRCNN based method, which is proposed in the original paper of SlowFast networks [3], and ACRN [44]. The backbone network of the above two methods is SlowFast\_8x8\_ResNet50. The pre-trained models are also provided by MMAction2 framework [83].

In Tab. 1, we summarize the baseline models and their performances on the original dataset, *i.e.*, the oracle performance.

## 4.4 Training Details

Under the blind setting, we perform self-supervised training for the proposed Dual-PVC framework with 60k unlabeled videos, which

Recognition Model	Dataset	Top1	Top5
TSM	UCF101	93.97	99.63
	HMDB51	72.81	92.88
	Kinetics400	70.73	89.81
	SomethingV1	47.85	76.78
	Diving48	75.99	97.16
TSM-16F	UCF101	94.45	99.39
	HMDB51	69.80	90.00
SlowOnly	UCF101	90.40	99.13
	HMDB51	63.53	89.67
	Kinetics400	71.22	87.57
TimeSformer	UCF101	95.43	99.63
	HMDB51	71.44	92.68
Detection Model	Dataset	mAP@0.5IoU	
SlowFast	AVA2.1 $^\diamond$	23.97	
ACRN	AVA2.1 $^\diamond$	25.74	

TABLE 1: Oracle performance of the evaluated baseline models.

are randomly sampled from the Kinetics dataset [9]. It should be emphasized here that we do not use any annotation of these videos. To accelerate the training procedure, the compressed videos  $\tilde{X}$  in Fig. 2 are pre-produced by performing compression followed by decompression operations on the original video, where the Constant Rate Factor (CRF) is set to 47 or 51 and we randomly adopt one from the videos processed by the two CRFs.  $\alpha$ ,  $\lambda$  and  $\tau$  are set to 0.1, 1, and 0.2, respectively. During optimization, we use the Adam optimizer [84] by setting the learning rate as 0.0001,  $\beta_1$  as 0.9 and  $\beta_2$  as 0.999, respectively. The resolution of training images is  $224 \times 224$  and the video clip length is 8. The temporal sampling strategy during training follows that of TSN [2], *i.e.*, we randomly sample 1 frame every 1 segment. It is worth mentioning here that the trained model can be applied to videos of any spatial resolution and temporal length, due to its fully convolutional characteristic. The training iteration number is 500k. The mini-batch size is 24. The whole system is implemented based on Pytorch [85] and it takes about 5 days to train the whole network using eight Nvidia 2080Ti GPUs.

We also introduce a *warm-start* stage before the regular training procedure stated above, as we find that directly optimizing through Eq. (8) renders the Enc-Net falling into a trivial solution: the perceptual feature  $\mathcal{S}$  is a constant all-zero tensor. Therefore, in the first 10k iterations, we replace the perceptual losses with MSE loss to warm-start the learning of Enc-Net.

Under the customized setting, the learning rate of the Adam optimizer is decayed by half, *i.e.*, 0.00005. The other hyperparameters are the same as those under the blind setting.

## 4.5 Evaluation Details

To give a fair comparison, both the bit cost of H.264 codec and our framework are computed online for the sampled clips during evaluation, following the official sampling protocol of the different video understanding methods. To measure the number of bits for encoding the representations, we use bits per pixel (Bpp) to represent the required bits for each pixel of the clip.

For the evaluation of the vanilla H.264 codec under different bitrate levels, the CRF value is selected from {47,43,39,35}. A larger CRF value leads to a lower bitrate. For our framework, the CRF value of the embedded H.264 codec is selected from {51,47,43,39}. The bitrate range of the H.264 codec in our framework is offset slightly lower than that of the vanilla H.264

Action Model	Dataset	BD-Top1	BD-Top5	BDBR(Top1)	BDBR(Top5)
TSM	UCF101	13.61	5.90	-37.92	-47.83
	HMDB51	20.07	16.33	-56.39	-50.32
	Kinetics400	21.15	21.14	-45.51	-44.49
	SomethingV1	6.34	6.22	-20.64	-18.61
	Diving48	6.02	5.00	-17.48	-17.73
TSM-16F	UCF101	6.11	2.03	-27.97	-30.49
	HMDB51	11.22	6.61	-30.19	-31.72
SlowOnly	UCF101	3.22	0.42	-18.12	-18.58
	HMDB51	2.39	1.44	-9.95	-16.43
	Kinetics400	7.91	7.18	-20.33	-20.65
TimeSformer	UCF101	2.13	2.88	-12.89	-5.26
	HMDB51	6.22	5.43	-23.67	-37.26

TABLE 2: BD-Accuracy and BDBR(Accuracy) performances of the proposed Dual-PVC framework in blind mode when compared with baseline H.264 codec. BD-Top1/BDBR(Top1) indicate the averagely improved Top1 accuracy and reduced bit cost percentage, respectively.

codec, so that the framework bitrate (H.264 stream+Perceptual stream) range can be roughly consistent with H.264. This is just for producing aesthetically pleasing rate-perception curves.

The compression efficiency of the H.264 codec is influenced by the sampling rate, especially by the sparse sampling strategy adopted by the downstream models. Nevertheless, we want to mention that our comparison scheme is indeed fair for the following two reasons: (1) real-world video understanding systems are also usually conducted on sparsely sampled clips, instead of the dense video clips. For example, we can let the H.264 video stream transport every frame, while only encoding the structure stream for some sparsely sampled frames for video understanding tasks. (2) We test upon different methods, which actually cover the sampling strategies from *sparse* to *dense*. For example, TSM sparsely samples 8 or 16 frames clip from a short video, SlowOnly network samples 1 frame very 4 consecutive frames, and SlowFast network densely samples every frame.

#### 4.6 Results on Action Recognition

**Blind mode.** We first analyze the improvement of the proposed Dual-PVC framework in the blind mode, which is friendly to deployment as it does not require fine-tuning the framework with downstream action recognition models. In other words, a blind Dual-PVC model can be directly applied to various pre-trained downstream models without the adaptation procedure such as fine-tuning. We report the improvement of recognition accuracy and the reduction of bit cost of the Dual-PVC framework compared with the vanilla H.264 codec, on the UCF101, HMDB51, Kinetics400, SomethingV1 and Diving48 datasets. The comparison results are calculated by the methods in Bjøntegaard Delta (BD) [86], which are widely adopted by previous works on video compression. The only difference is that we replace the performance metric from PSNR/SSIM to Top1/Top5 accuracy.

In Tab. 2, we can clearly observe that our framework outperforms the baseline ‘‘H.264 plus action recognition’’ by a large margin in terms of all settings. For example, on the setting of ‘‘HMDB51 dataset+TSM model’’, when compared to the baseline H.264 codec, our method averagely boosts the accuracy by 20.07% in terms of Top1 accuracy, yet averagely reducing the bit cost by 56.39% for achieving the same performance. The good results over these settings reveal two advantages of the proposed framework: (1) **Strong generality on various datasets and models.** (2) **Effective with different frame sampling strategies,** from the sparse TSN-style strategy adopted by TSM network to the dense

sampling strategy adopted by SlowOnly network. The dense sampling strategy is responsible for the relatively small improvements of our framework on the SlowOnly network results. A similar performance drop can be also observed by comparing the results of the 8 frames TSM model (denoted as TSM) and the 16 frames TSM model (denoted as TSM-16F), because the sampling rate of the latter is two times higher than the former.

**Customized mode.** Although our framework has achieved impressive performance on the blind mode, we can further improve the performance of the whole system by jointly optimizing it with the downstream models. As shown in Tab. 3, finetuning Dual-PVC framework with the downstream models significantly improves the performance. For example, the improvement of the SlowOnly model is 2.61% in terms of BD-Top1.

TSM	BD-Top1	BD-Top5	BDBR(Top1)	BDBR(Top5)
Blind	13.61	5.90	-37.92	-47.83
<b>Customized</b>	<b>15.94</b>	<b>6.28</b>	<b>-40.23</b>	<b>-48.14</b>
$\Delta$	2.33 $\uparrow$	0.38 $\uparrow$	-2.31 $\downarrow$	-0.31 $\downarrow$
SlowOnly	BD-Top1	BD-Top5	BDBR(Top1)	BDBR(Top5)
Blind	3.22	0.42	-18.12	-18.58
<b>Customized</b>	<b>5.83</b>	<b>1.27</b>	<b>-21.86</b>	<b>-19.01</b>
$\Delta$	2.61 $\uparrow$	0.85 $\uparrow$	-3.74 $\downarrow$	-0.43 $\downarrow$

TABLE 3: The BD-Accuracy and BDBR(Accuracy) performances of Dual-PVC framework in customized mode on UCF101, when using H.264 codec as the anchor. We also give the performance gains of the customized mode over the blind mode.

**Rate Performance (RP)-curves.** We also illustrate the RP-curves in Fig. 5, in which Top1 accuracy and bit per pixel (bpp) are adopted as the performance metric and the bit cost metric. Several critical findings can be immediately observed:

(1) **Dual-PVC is stable across various bitrate levels.** We first see that the action recognition performances are consistently improved across all bitrates on every model and every dataset, although our framework is only trained on the videos pre-compressed with two bitrate levels. More importantly, the lower bitrate, the larger performance gain. For example, under 0.08bpp bit cost level, our framework achieves 86% top1 accuracy while the prediction accuracy with using vanilla H.264 codec is about only 62%, which is a substantial improvement (24% in terms of Top1 accuracy). We also summarize the performance gain under low bitrate levels in Tab. 4. The proposed dual-bitstream framework always significantly outperforms the single-stream H.264



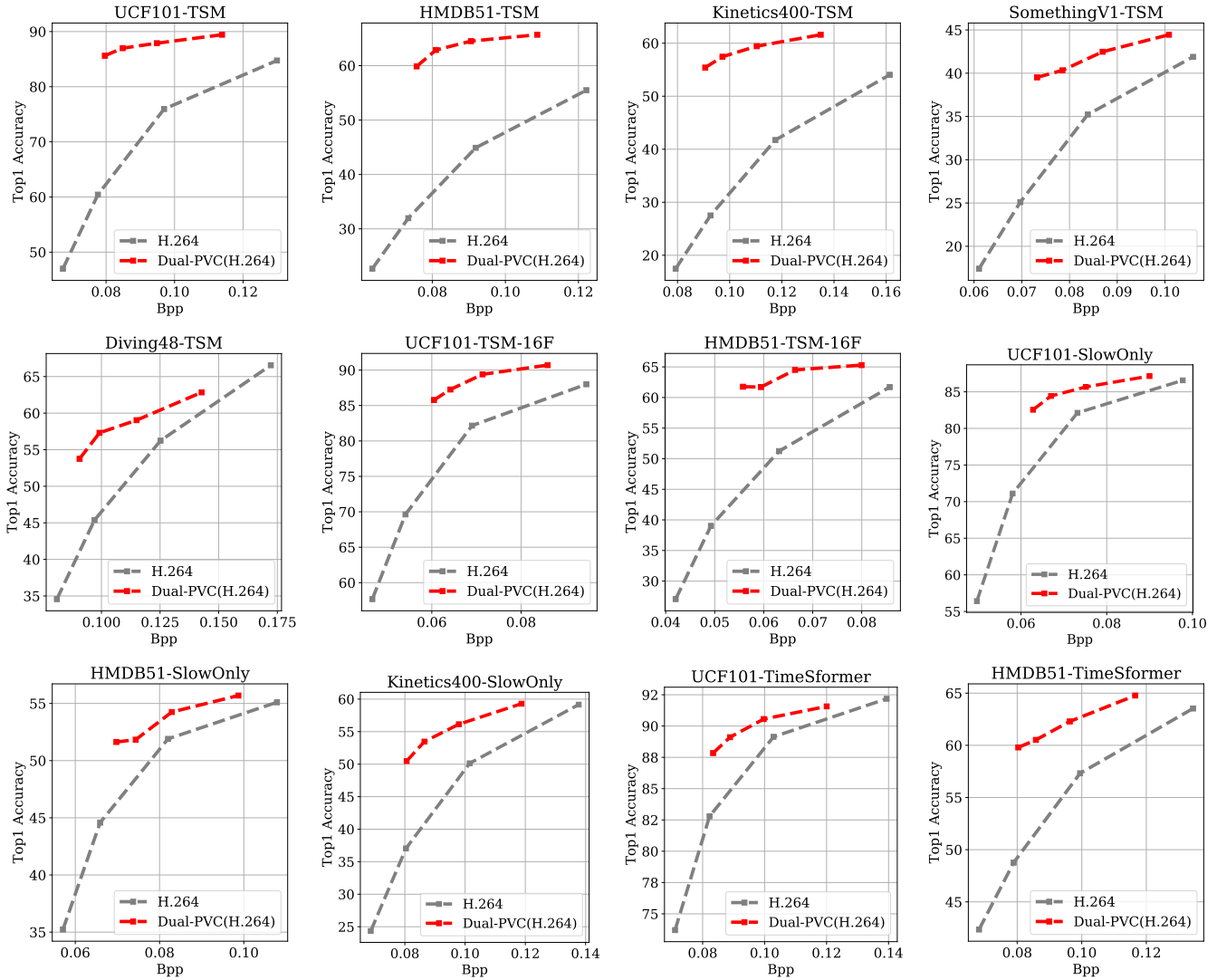


Fig. 5: Comparison between the proposed Dual-PVC framework in *blind* mode and the vanilla H.264 codec on action recognition task. Notably, only a single model is trained and directly evaluated on all datasets and models.

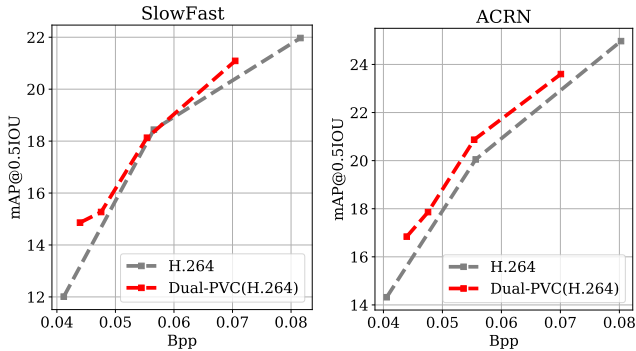


Fig. 6: Comparison between the proposed Dual-PVC framework in *blind* mode and the vanilla H.264 codec on action detection task.

codec. The capability of reliably recognizing the very low bit-rate videos renders the deployment of intelligent surveillance systems possible in poor network connection scenarios.

(2) *Dual-PVC performs better on appearance-biased datasets.* We take the TSM model for example, of which results

Dataset	Bpp	Top1 (H.264)	Top1 (Dual-PVC)	$\Delta$ Top1 $\uparrow$
UCF101	0.080	61.23	<b>85.86</b>	24.63
HMDB51	0.077	37.19	<b>62.91</b>	25.71
Kinetics400	0.092	27.93	<b>52.95</b>	25.02
SomethingV1	0.072	27.38	<b>39.84</b>	12.46
Diving48	0.096	41.76	<b>53.46</b>	11.70

TABLE 4: The performance gain of the Dual-PVC framework over the H.264 baseline under low bitrate levels.

are shown in the first six plots of Fig. 5. It is clear that the performance improvements are relatively large on appearance-biased such as UCF101, HMDB51 and Kinetics400, compare with motion-biased datasets such as Something V1 and Diving48, especially at very low bit cost levels. A similar trend can also be concluded from the results in Tab. 2 and Tab. 4. The reasons are in two aspects. First, the frames of motion-biased datasets are with relatively simple textures, which are easier for traditional video codecs to compress. Note that video codecs such as H.264 are very efficient in compressing motion information. Second, the Dual-PVC framework mainly focuses on compensating or correcting the structures of the video frames instead of refining motion



Fig. 7: Restored frames by our Dual-PVC framework. We report the bit cost (in bpp), the quality (in PSNR/SSIM/FID) and the recognition result, respectively. The wrongly recognized action category is in red color, while the correct one is in green color. Higher PSNR/SSIM or lower FID denote better video quality. Lower bpp denotes more bit cost saved. *Best to view by zooming-in.*

information. We also mention here that most actions involved in the practical surveillance systems are appearance-biased. For example, recognizing different criminal actions largely relies on finding out the discriminative murder weapons.

(3) **The robustness of Transformers to compression artifacts is better than CNNs.** For example, the performance drops of TimeSformer and TSM are about 8% and 18% in terms of Top1 accuracy, when the bit costs are reduced from 0.10bpp to 0.08bpp. We think the reason is that the Transformers leverage the global information for prediction while the CNNs mostly rely on local texture cues.

#### 4.7 Results on Action Detection

We illustrate the RP-curves of SlowFast network and ARCNet in Fig. 6, where the mAP@0.5IoU is used as the performance metric. Our framework outperforms the baseline method (H.264 codec) over all bitrate levels. The relatively marginal improvements compared to the action recognition task may be ascribed to two reasons. First, the action categories in the AVA dataset are quite fine-grained, which require comprehensively reasoning the human-context, human-human and human-context-human interactions to recognize. Thus, the action detection models trained on it are more vulnerable/in-robust to the minor domain gap between the restored videos by our framework and the original video. Note

that we do not adapt the action detection model to the Dual-PVC framework by jointly fine-tuning. Second, the adopted action detection methods are in a two-stage scheme, *i.e.*, actor detection followed by action classification. The misalignment between the pre-calculated actor bounding box on the original dataset and the restored videos by our method also renders the cropped feature by RoI-Align operation inaccurate.

#### 4.8 Visualization of the Restored Videos

As shown in Fig. 7, we demonstrate the restoration results of the videos, which are randomly selected from the kinetics400 validation set. It is clear that the blocking artifacts caused by video compression are largely eliminated by our framework. Additionally, the restored videos demonstrate two main characteristics: (1) visually pleasant and full of sharp edges and (2) preserving the object structures that are essential to video understanding.

In Fig. 7, we also report the quantitative quality of the restored videos in terms of PSNR, SSIM [16] and FID [87]. The first two metrics are used to measure the low-level similarity of the video content, while the last one calculates the similarity between the distributions of the ground-truth and generated frames. We find that the PSNR/SSIM of the videos by Dual-PVC is a little bit lower than H.264 codec under the similar bpp level, but the distribution of the frames by Dual-PVC is more closed to the ground-truth

when using the FID as the metric. This observation is consistent with the previous finding that FID is more suitable for serving as a perceptual metric for visual quality [87].

### 5 FRAMEWORK ANALYSIS

In this section, we take the action recognition task as the example, and perform extensive experiments to investigate every aspect of the proposed Dual-PVC framework by answering the following questions. In all experiments, the action recognition model is TSM and the dataset is UCF101, if not otherwise specified.

**Q1: Are the introduced perceptual stream necessary?** To answer this question, we remove the perceptual stream within the framework. This degenerates to a “video restoration+video understanding” paradigm, which is called *Obit* variant, since we do not need to transport any extra bits here.

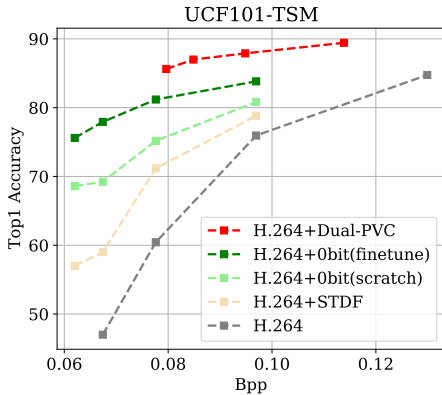


Fig. 8: The results of *Obit* model, in which the perceptual stream is removed. “scratch” and “finetune” denote training from scratch and initializing from the Dual-PVC framework, respectively.

As shown in Fig. 8, we first try to train the *Obit* model from scratch, which is denoted as “H.264+0bit(scratch)” in the figure. It is surprising that the recognition accuracy can be hugely improved by over 20% without introducing any extra bitrate, although it is still rather inferior to the dual-bitstream Dual-PVC framework. We conclude the improvements are raised from the fact that our video enhancement network R-Net corrects the compressed video distribution to that of natural videos, which immediately repairs the easy negative samples. Similar findings are also observed by previous works [88] on GAN-based facial image enhancement, which adopts similar loss items to our method, *i.e.*, the perceptual loss and the GAN loss. We also try to train another *Obit* model by fine-tuning the R-Net of the pre-trained Dual-PVC framework, denoted as “H.264+0bit (finetune)”. The performance of it is much better than “H.264+0bit (scratch)”, although all settings of the two models are consistent other than the initialization strategy of R-Net. The superior performance of the *Obit*(finetune) model indicates that the Dual-PVC framework can largely improve the compressed video understanding tasks without introducing any extra bit costs and computation cost on edge devices, which is very friendly to the practical deployment.

To summarize, the dual-bitstream design, *i.e.*, the introduction of the perceptual stream, is the key to a high-performance compressed video understanding framework. Even we do not use it in the deployment stage, optimizing with it in the pretraining stage can still substantially improve the performance.

Besides, we also train a recent compressed video quality enhancement network STDF [53] using the same training data

as our model. Action recognition results on the enhanced videos by STDF indeed perform better than H.264 baseline, but much inferior to the 0bit model equipping with R-Net, as shown in the yellow curve of Fig. 8. For example, at the  $\sim 0.06\text{bpp}$  bitrate level, the top1 accuracy drops about 20%. This strongly justifies the network designs of R-Net, *i.e.*, enhancement in low-resolution space and adaptive fusion module, are effective for video perceptual coding.

Finally, we give a comparison of the bits cost by the perceptual stream and the video stream, as shown in Tab. 5. The perceptual stream only occupies a small proportion of the whole bit cost. Notably, on the large-scale Kinetics400 dataset, only 12% of the network traffic is consumed by our perceptual stream.

Dataset	Bpp	Bpp(S)	Percentage(S)
UCF101	0.1138	0.0169	14%
HMDB51	0.1087	0.0168	15%
Kinetics400	0.1349	0.0173	12%
SomethingV1	0.1008	0.0170	16%
Diving48	0.1427	0.0175	12%

TABLE 5: The absolute bit cost and the relative percentage of the perceptual stream  $\mathcal{S}$ . The values are evaluated with the CRF of the embedded H.264 codec set to 39.

**Q2: Is the proposed edge map-based perceptual loss effective?** In this section, we remove  $\mathcal{L}_{edge}$  to study the effectiveness of the proposed assumption, *i.e.*, if  $\mathcal{L}_{edge}$  is a good perceptual loss for compressed video understanding. We name the produced variant model “woEdge”.

Bpp	0.08	0.09	0.10	0.11
woEdge	82.2	85.5	87.1	88.6
Sobel Extractor	82.4	85.8	87.5	88.6
<b>Dual-PVC(Edge-Net)</b>	<b>85.3</b>	<b>87.6</b>	<b>88.1</b>	<b>89.4</b>

TABLE 6: Comparison of Top1 accuracy of models trained with different edge map constraints. The Sobel edge extractor improves the baseline “woEdge” model marginally. In contrast, the edge extracted by the adopted learnable Edge-Net significantly benefits the framework over all bitrate levels.

As shown in Tab. 6, the Top1 accuracy of the woEdge model drops by  $\sim 3\%$  at the 0.08bpp level, compared to the full Dual-PVC framework optimized with  $\mathcal{L}_{edge}$ . Moreover, we find that the performance gap is shrunk at the higher bpp level. For example, the performance gap is only 0.8% at the 0.11bpp level. The reason is that the object edges/structures are corrupted heavily under the large compression ratio. Furthermore, we train a model by replacing the learnable Edge-Net with a hand-crafted edge extractor Sobel filter, the performance is also decreased drastically, proving that a learnable edge extractor is necessary for a superior perceptual video coding framework.

$\alpha$	0	0.001	0.01	0.1	1
Dual-PVC	82.2	83.9	85.3	85.5	80.8

TABLE 7: Impact of the loss weight  $\alpha$  in terms of Top1 accuracy. The target bitrate is 0.08bpp.

Then, we analyze the impact of the weight  $\alpha$  for  $\mathcal{L}_{edge}$ , as shown in Tab. 7. The performance increases consistently with the larger  $\alpha$ . Although the performance of  $\alpha = 0.1$  is a little bit higher than that of  $\alpha = 0.01$ , we still adopt  $\alpha = 0.01$  due to its smaller

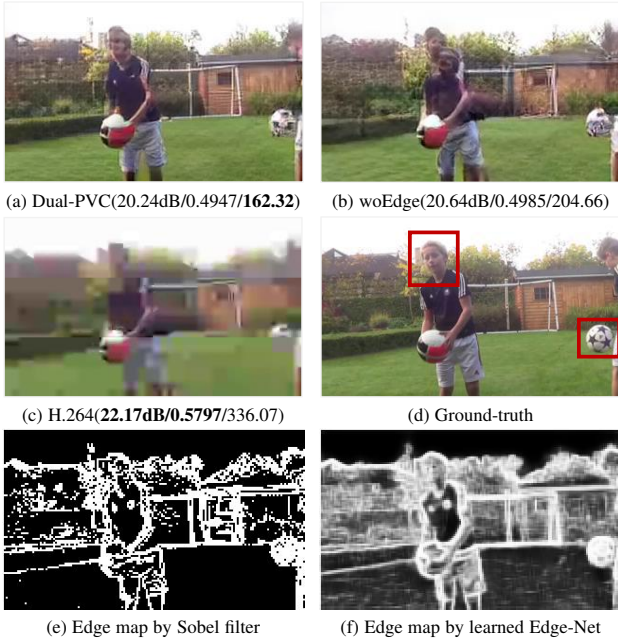


Fig. 9: Visualization of the decoded videos of different models. Dual-PVC demonstrates much better visual quality compared to the woEdge model and the baseline H.264 codec. We also report the quantitative quality results (PSNR/SSIM/FID). Besides, the edge maps produced by Sobel filter and our method are shown in (e) and (f), respectively. The video is randomly sampled from the category *Juggling Soccer Ball* of Kinetics validation set. *Best to view by zooming in.*

validation performance variance of different epochs. When  $\alpha$  is set to a very large value,  $\alpha = 1$ , the performance is suddenly decreased due to the instability of the training procedure.

To give a more intuitive understanding, we further compare the reconstructed video frames with/without  $\mathcal{L}_{edge}$ , as shown in Fig. 9. We first observe that the reconstructed frames by our methods, *i.e.*, (a) and (b), both depict sharp edges, due to the adoption of the GAN loss. However, without the edge loss, the frame rendered by woEdge model is far away from the ground-truth frame in terms of the object structures. For example, the shoulder of the human and the football in the background are severely distorted, which causes the downstream action recognition model mis-classifying the video from *Juggling Soccer Ball* to *Shooting Basketball*.

We also compare the edge maps produced by the hand-crafted Sobel filter and our learnable Edge-Net, as shown in the last row of Fig. 9. Compared to the Sobel filter, our edge map is much consistent with the human perception and clearly show some critical visual elements beneficial for recognition, such as human, ball and buildings. Note that our method is only learned from the raw videos by contrastive learning objective, without leveraging the external perceptual edge map datasets such as BSDS500 [89]. The perceptually good edge map facilitates the preservation of key object structures within the decoded frames, as shown in Fig. 9 (a).

**Q3: Is the LPIPS loss better than low-level metrics for constraining the local color distribution?** In the previous question, we answer the necessity of the edge loss to a high-performance compressed video understanding framework. However, it is only responsible for the object contours instead of the local texture structures. Therefore, we also incorporate the LPIPS loss  $\mathcal{L}_{lrips}$  into the loss function, aiming to regularize the local color distribution. In this section, we investigate the advantage of  $\mathcal{L}_{lrips}$  over the traditional color constraints, *i.e.*, PSNR and SSIM [90].

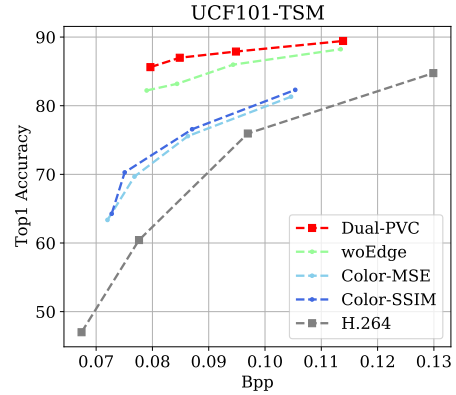


Fig. 10: Ablation on the loss function in Eq.(8). “woEdge” denotes removing  $\mathcal{L}_{edge}$ . “Color-MSE” and “Color-SSIM” denote replacing  $\mathcal{L}_{lrips}$  with MSE loss and SSIM loss, respectively.

Specifically, we train another two models by replacing  $\mathcal{L}_{lrips}$  with the two metrics above, which are widely used as the distortion loss item in the previous learnable video compression methods. We denote the two models as “Color-MSE” and “Color-SSIM”. As shown in Fig. 10, both of them are much inferior to the original Dual-PVC model, which adopts the perceptual loss. The large performance drops are reasonable, because the two losses are low-level pixel-wise metrics, which facilitate the learning of the texture details instead of the semantics-rich structures. In contrast, the perceptual loss is pre-trained with the human perceptual evaluation scores, which are more consistent with our downstream tasks, *i.e.*, the video understanding tasks.

**Q4: Are the adaptive compression designs in Enc-Net necessary?** As mentioned in section 3.1, Enc-Net is adaptive to either the codec or the current input videos. To verify the effectiveness of these designs, we change the network architecture of Enc-Net, then evaluate the models with the H.264 codec (with CRF=51).

Diff-Map	Kernel Strategy	bpp(S) $\times 10^{-2}$	Top1 %
✗	AdaKT+AdaKM	2.45	85.12
✓	Plain Conv	2.09	84.85
✓	FixKT+AdaKM	1.92	85.62
✓	<b>AdaKT+AdaKM</b>	<b>1.76</b>	<b>85.63</b>

TABLE 8: Ablation studies of Enc-Net. “AdaKT”/“FixKT” represents the kernel table is adaptive to the input video or fixed. “Plain Conv” denotes the adaptive convolution is replaced with a plain group-wise convolution. “✗ Diff-Map” denotes the difference map pathway is removed. We only show the bit cost of the perceptual stream  $\mathcal{S}$ , since the video stream cost of these models is the same.

The results are shown in Tab. 8. When removing the difference map pathway, the bit cost of the perceptual stream is substantially increased by  $\sim 35\%$ . In this situation, the perceptual stream is no longer adaptive to the video stream produced by the video codec. Therefore, the information already encoded by the video stream may be repetitively packaged into the perceptual stream. Besides, removing this pathway also cut the parameter number of Enc-Net by  $\sim 10\%$ , which also elicits the reduction of compression efficiency. We also investigate the impact of the adaptive convolution design adopted by the feature fusion module D-GFM. Remember that we synthesize the convolution kernels via indexing the adaptive kernel table(AdaKT) with an adaptive kernel index map(AdaKM). When replacing the video instance-adaptive AdaKT with the fixed kernel table (FixKT), which is shared by all videos, the performances are obviously degraded in terms of both

bit cost and recognition accuracy. Finally, we adopt a simple plain convolution to extract the perceptual stream, the performance is further reduced. However, it is still better than the single pathway architecture, though. From the analysis above, we can conclude that all designs for adaptive compression within Enc-Net benefit the overall performance.

## 6 FLEXIBLE EXTENSION FOR DUAL-PVC MODEL

Our framework is very flexible and other modern techniques can be readily used to improve the submodules of our Dual-PVC model. For example, the multi-head self-attention (MHSA) module borrowed from Transformer [74] can be adopted in the Enc-Net and R-Net, for achieving a better trade-off between the computation cost and the video reconstruction quality. The hyper-prior model [67] can be introduced to improve the compression efficiency of the perceptual stream. The H.264 codec can also be replaced with more advanced video codecs such as H.265 [56].

We take the third extension, *i.e.*, upgrading the embedded video codec as an example. The results are shown in Tab. 9. When the codec is upgraded from H.264 to H.265, the performance of Dual-PVC is further significantly improved, 14.47% and 8.72% in terms of Top1 and Top5 accuracy.

Model	BD-Top1	BD-Top5	BDBR(Top1)	BDBR(Top5)
Dual-PVC(H.264)	13.61	5.90	-37.92	-47.83
<b>Dual-PVC(H.265)</b>	<b>28.08</b>	<b>14.62</b>	<b>-50.57</b>	<b>-47.87</b>
$\Delta$	14.47 $\uparrow$	8.72 $\uparrow$	-12.65 $\downarrow$	-0.04 $\downarrow$

TABLE 9: Our Dual-PVC framework can be further improved by using a more advanced H.265 video codec.

## 7 COMPLEXITY ANALYSIS

We evaluate the computational complexity of our framework with an input video clip of spatial scale  $224 \times 224$ , which is the standard resolution adopted by most video understanding methods.

Model	Side	Parameters(M)	FLOPs(G)
Enc-Net	Edge	7.0	<b>1.1</b>
R-Net	Cloud	6.2	3.9
Balle <i>et al.</i> [67]	Edge	11.8	19.8

TABLE 10: The trainable parameters and FLOPs for the networks within the proposed Dual-PVC. FLOPs indicates the computational cost for encoding a single frame of size  $224 \times 224$ .

As shown in Tab. 10, our architecture demonstrates a *light edge yet heavy cloud* scheme in terms of FLOPs, which conforms to the fact that the computational resources on edge devices are usually limited. We also give the complexity of the representative work on learnable image compression, *i.e.*, Balle *et al.* [67]. Our Enc-Net architecture saves the edge-side computational cost by about 20 times, which makes our framework possible for practical deployment. We also emphasize that our 0bit model also achieves superior performance, as shown in Fig. 8. This model introduces *zero* complexity to edge devices.

## 8 CONCLUSION

In this paper, we have proposed a dual-stream perceptual coding framework Dual-PVC for compressed video understanding. Our framework inherits the advantages of both efficient content-coding

capability of traditional video codecs and flexible perceptual coding of neural networks. Experimental results show that our approach outperforms the widely used H.264 codec by a large margin on downstream video understanding tasks, *i.e.*, action recognition and action detection. Moreover, we have built a benchmark for this novel problem.

## REFERENCES

- [1] D. Tran, L. Bourdev, R. Fergus, L. Torresani, and M. Paluri, "Learning spatiotemporal features with 3d convolutional networks," in *ICCV*, 2015.
- [2] L. Wang, Y. Xiong, Z. Wang, Y. Qiao, D. Lin, X. Tang, and L. Van Gool, "segment networks: Towards good practices for deep action recognition," in *ECCV*, 2016.
- [3] C. Feichtenhofer, H. Fan, J. Malik, and K. He, "Slowfast networks for video recognition," in *ICCV*, 2019.
- [4] J. Lin, C. Gan, and S. Han, "Tsm: temporal shift module for efficient video understanding," in *ICCV*, 2019.
- [5] Y. Li, B. Ji, X. Shi, J. Zhang, B. Kang, and L. Wang, "Tea: Temporal excitation and aggregation for action recognition," in *CVPR*, 2020.
- [6] Y. Li, Z. Wang, L. Wang, and G. Wu, "Actions as moving points," in *ECCV*, 2020.
- [7] H. Kuehne, H. Jhuang, E. Garrote, T. Poggio, and T. Serre, "Hmdb: a large video database for human motion recognition," in *ICCV*. IEEE, 2011.
- [8] K. Soomro, A. R. Zamir, and M. Shah, "Ucf101: A dataset of 101 human actions classes from videos in the wild," *arXiv preprint arXiv:1212.0402*, 2012.
- [9] J. Carreira and A. Zisserman, "Quo vadis, action recognition? a new model and the kinetics dataset," in *CVPR*, 2017.
- [10] R. Goyal, S. E. Kahou, V. Michalski, J. Materzynska, S. Westphal, H. Kim, V. Haenel, I. Freund, P. Yianilos, M. Mueller-Freitag *et al.*, "The" something something" video database for learning and evaluating visual common sense," in *ICCV*, 2017.
- [11] Y. Li, Y. Li, and N. Vasconcelos, "Resound: Towards action recognition without representation bias," in *ECCV*, 2018.
- [12] C. Yi, S. Yang, H. Li, Y.-p. Tan, and A. Kot, "Benchmarking the robustness of spatial-temporal models against corruptions," *NIPS*, 2021.
- [13] R. Pourreza, A. Ghodrati, and A. Habibi, "Recognizing compressed videos: Challenges and promises," in *ICCVW*, 2019.
- [14] Y. Blau and T. Michaeli, "Rethinking lossy compression: The rate-distortion-perception tradeoff," in *ICML*, 2019.
- [15] C. E. Shannon, "A mathematical theory of communication," *The Bell system technical journal*, 1948.
- [16] Z. Wang, A. C. Bovik, H. R. Sheikh, and E. P. Simoncelli, "Image quality assessment: from error visibility to structural similarity," *TIP*, 2004.
- [17] J. Ballé, V. Laparra, and E. P. Simoncelli, "End-to-end optimized image compression," *arXiv*, 2016.
- [18] S. Liu and A. C. Bovik, "Efficient dct-domain blind measurement and reduction of blocking artifacts," *CSVT*, 2002.
- [19] T. Meier, K. N. Ngan, and G. Crebbin, "Reduction of blocking artifacts in image and video coding," *CSVT*, 1999.
- [20] H.-S. Kong, A. Vetro, and H. Sun, "Edge map guided adaptive post-filter for blocking and ringing artifacts removal," in *IISCS*, 2004.
- [21] K. Nazeri, E. Ng, T. Joseph, F. Z. Qureshi, and M. Ebrahimi, "Edgeconnect: Generative image inpainting with adversarial edge learning," *arXiv*, 2019.
- [22] I. H. Witten, R. M. Neal, and J. G. Cleary, "Arithmetic coding for data compression," *Communications of the ACM*, 1987.
- [23] G. Bertasius, H. Wang, and L. Torresani, "Is space-time attention all you need for video understanding?" *arXiv*, 2021.
- [24] B. Zhang, L. Wang, Z. Wang, Y. Qiao, and H. Wang, "Real-time action recognition with enhanced motion vector cnns," in *CVPR*, 2016.
- [25] C.-Y. Wu, M. Zaheer, H. Hu, R. Manmatha, A. J. Smola, and P. Krähenbühl, "Compressed video action recognition," in *CVPR*, 2018.
- [26] Z. Shou, X. Lin, Y. Kalantidis, L. Sevilla-Lara, M. Rohrbach, S.-F. Chang, and Z. Yan, "Dmc-net: Generating discriminative motion cues for fast compressed video action recognition," in *CVPR*, 2019.
- [27] Y. Huo, M. Ding, H. Lu, N. Fei, Z. Lu, J.-R. Wen, and P. Luo, "Compressed video contrastive learning," *NIPS*, 2021.
- [28] K. Simonyan and A. Zisserman, "Two-stream convolutional networks for action recognition in videos," in *NIPS*, 2014.
- [29] C. Feichtenhofer, A. Pinz, and A. Zisserman, "Convolutional two-stream network fusion for video action recognition," in *CVPR*, 2016.

- [30] L. Wang, Y. Xiong, Z. Wang, Y. Qiao, D. Lin, X. Tang, and L. Van Gool, "Temporal segment networks for action recognition in videos," *TPAMI*, 2018.
- [31] B. Zhou, A. Andonian, A. Oliva, and A. Torralba, "Temporal relational reasoning in videos," in *ECCV*, 2018.
- [32] Z. Liu, D. Luo, Y. Wang, L. Wang, Y. Tai, C. Wang, J. Li, F. Huang, and T. Lu, "Teinet: Towards an efficient architecture for video recognition," in *AAAI*, 2020.
- [33] L. Wang, Z. Tong, B. Ji, and G. Wu, "Tdn: Temporal difference networks for efficient action recognition," in *CVPR*, 2021.
- [34] Z. Liu, L. Wang, W. Wu, C. Qian, and T. Lu, "Tam: Temporal adaptive module for video recognition," in *ICCV*, 2021.
- [35] Y. Tian, X. Min, G. Zhai, and Z. Gao, "Video-based early asd detection via temporal pyramid networks," in *ICME*, 2019.
- [36] K. Hara, H. Kataoka, and Y. Satoh, "Learning spatio-temporal features with 3d residual networks for action recognition," in *ICCVW*, 2017.
- [37] Y. Tian, Z. Che, W. Bao, G. Zhai, and Z. Gao, "Self-supervised motion representation via scattering local motion cues," in *ECCV*, 2020.
- [38] D. Tran, H. Wang, L. Torresani, J. Ray, Y. LeCun, and M. Paluri, "A closer look at spatiotemporal convolutions for action recognition," in *CVPR*, 2018.
- [39] Z. Qiu, T. Yao, and T. Mei, "Learning spatio-temporal representation with pseudo-3d residual networks," in *ICCV*, 2017.
- [40] C. Feichtenhofer, "X3d: Expanding architectures for efficient video recognition," in *CVPR*, 2020.
- [41] C. Szegedy, S. Ioffe, V. Vanhoucke, and A. A. Alemi, "Inception-v4, inception-resnet and the impact of residual connections on learning," in *AAAI*, 2017.
- [42] K. He, X. Zhang, S. Ren, and J. Sun, "Deep residual learning for image recognition," in *CVPR*, 2016.
- [43] J. Deng, W. Dong, R. Socher, L.-J. Li, K. Li, and L. Fei-Fei, "Imagenet: A large-scale hierarchical image database," in *CVPR*, 2009.
- [44] C. Sun, A. Shrivastava, C. Vondrick, K. Murphy, R. Sukthankar, and C. Schmid, "Actor-centric relation network," in *ECCV*, 2018.
- [45] J. Pan, S. Chen, M. Z. Shou, Y. Liu, J. Shao, and H. Li, "Actor-context-actor relation network for spatio-temporal action localization," in *CVPR*, 2021.
- [46] C.-Y. Wu, C. Feichtenhofer, H. Fan, K. He, P. Krahenbuhl, and R. Girshick, "Long-term feature banks for detailed video understanding," in *CVPR*, 2019.
- [47] J. Wu, Z. Kuang, L. Wang, W. Zhang, and G. Wu, "Context-aware rnn: A baseline for action detection in videos," in *ECCV*.
- [48] O. Köpüklü, X. Wei, and G. Rigoll, "You only watch once: A unified cnn architecture for real-time spatiotemporal action localization," *arXiv*, 2019.
- [49] T. Xue, B. Chen, J. Wu, D. Wei, and W. T. Freeman, "Video enhancement with task-oriented flow," *IJCV*, 2019.
- [50] G. Lu, W. Ouyang, D. Xu, X. Zhang, Z. Gao, and M.-T. Sun, "Deep kalman filtering network for video compression artifact reduction," in *ECCV*, 2018.
- [51] R. Yang, M. Xu, Z. Wang, and T. Li, "Multi-frame quality enhancement for compressed video," in *CVPR*, 2018.
- [52] Y. Jo, S. W. Oh, J. Kang, and S. J. Kim, "Deep video super-resolution network using dynamic upsampling filters without explicit motion compensation," in *CVPR*, 2018.
- [53] J. Deng, L. Wang, S. Pu, and C. Zhuo, "Spatio-temporal deformable convolution for compressed video quality enhancement," in *AAAI*, 2020.
- [54] J. Dai, H. Qi, Y. Xiong, Y. Li, G. Zhang, H. Hu, and Y. Wei, "Deformable convolutional networks," in *ICCV*, 2017.
- [55] T. Wiegand, G. J. Sullivan, G. Bjontegaard, and A. Luthra, "Overview of the h. 264/avc video coding standard," *TCSVT*, 2003.
- [56] G. J. Sullivan, J.-R. Ohm, W.-J. Han, and T. Wiegand, "Overview of the high efficiency video coding (hevc) standard," *TCSVT*, 2012.
- [57] G. Lu, W. Ouyang, D. Xu, X. Zhang, C. Cai, and Z. Gao, "Dvc: An end-to-end deep video compression framework," in *CVPR*, 2019.
- [58] J. Lin, D. Liu, H. Li, and F. Wu, "M-lvc: multiple frames prediction for learned video compression," in *CVPR*, 2020.
- [59] Z. Hu, Z. Chen, D. Xu, G. Lu, W. Ouyang, and S. Gu, "Improving deep video compression by resolution-adaptive flow coding," in *ECCV*, 2020.
- [60] R. Yang, F. Mentzer, L. V. Gool, and R. Timofte, "Learning for video compression with hierarchical quality and recurrent enhancement," in *CVPR*, 2020.
- [61] Z. Hu, G. Lu, and D. Xu, "Fvc: A new framework towards deep video compression in feature space," in *CVPR*, 2021.
- [62] J. Li, B. Li, and Y. Lu, "Deep contextual video compression," *NIPS*, 2021.
- [63] Y. Tian, G. Lu, X. Min, Z. Che, G. Zhai, G. Guo, and Z. Gao, "Self-conditioned probabilistic learning of video rescaling," in *ICCV*, 2021.
- [64] R. Yang, L. Van Gool, and R. Timofte, "Perceptual learned video compression with recurrent conditional gan," *arXiv*, 2021.
- [65] V. Nair and G. E. Hinton, "Rectified linear units improve restricted boltzmann machines," in *ICML*, 2010.
- [66] J. Hu, L. Shen, and G. Sun, "Squeeze-and-excitation networks," in *CVPR*, 2018.
- [67] J. Ballé, D. Minnen, S. Singh, S. J. Hwang, and N. Johnston, "Variational image compression with a scale hyperprior," *arXiv*, 2018.
- [68] D. Minnen, J. Ballé, and G. Toderici, "Joint autoregressive and hierarchical priors for learned image compression," *arXiv*, 2018.
- [69] H. Su, V. Jampani, D. Sun, O. Gallo, E. Learned-Miller, and J. Kautz, "Pixel-adaptive convolutional neural networks," *arXiv*, 2019.
- [70] O. Ronneberger, P. Fischer, and T. Brox, "U-net: Convolutional networks for biomedical image segmentation," in *MICCAI*, 2015.
- [71] B. Xu, N. Wang, T. Chen, and M. Li, "Empirical evaluation of rectified activations in convolutional network," *arXiv*, 2015.
- [72] M. Sandler, A. Howard, M. Zhu, A. Zhmoginov, and L.-C. Chen, "Mobilenetv2: Inverted residuals and linear bottlenecks," in *CVPR*, 2018.
- [73] G. Huang, Z. Liu, L. Van Der Maaten, and K. Q. Weinberger, "Densely connected convolutional networks," in *CVPR*, 2017.
- [74] A. Vaswani, N. Shazeer, N. Parmar, J. Uszkoreit, L. Jones, A. N. Gomez, L. Kaiser, and I. Polosukhin, "Attention is all you need," *arXiv*, 2017.
- [75] C. Lea, M. D. Flynn, R. Vidal, A. Reiter, and G. D. Hager, "Temporal convolutional networks for action segmentation and detection," in *CVPR*, 2017.
- [76] Z. Qiu, T. Yao, Y. Shu, C.-W. Ngo, and T. Mei, "Condensing a sequence to one informative frame for video recognition," in *ICCV*, 2021.
- [77] R. Zhang, P. Isola, A. A. Efros, E. Shechtman, and O. Wang, "The unreasonable effectiveness of deep features as a perceptual metric," in *CVPR*, 2018.
- [78] K. Simonyan and A. Zisserman, "Very deep convolutional networks for large-scale image recognition," *arXiv*, 2014.
- [79] P. Isola, J.-Y. Zhu, T. Zhou, and A. A. Efros, "Image-to-image translation with conditional adversarial networks," in *CVPR*, 2017.
- [80] J. H. Lim and J. C. Ye, "Geometric gan," *arXiv*, 2017.
- [81] C. Gu, C. Sun, D. A. Ross, C. Vondrick, C. Pantofaru, Y. Li, S. Vijayanarasimhan, G. Toderici, S. Ricco, R. Sukthankar *et al.*, "Ava: A video dataset of spatio-temporally localized atomic visual actions," in *CVPR*, 2018.
- [82] R. Girdhar, J. Carreira, C. Doersch, and A. Zisserman, "A better baseline for ava," *arXiv*, 2018.
- [83] M. Contributors, "Openmmlab's next generation video understanding toolbox and benchmark," <https://github.com/open-mmlab/mmaaction2>, 2020.
- [84] D. P. Kingma and J. Ba, "Adam: A method for stochastic optimization," *arXiv*, 2014.
- [85] A. Paszke, S. Gross, F. Massa, A. Lerer, J. Bradbury, G. Chanan, T. Killeen, Z. Lin, N. Gimelshein, L. Antiga *et al.*, "Pytorch: An imperative style, high-performance deep learning library," in *NIPS*, 2019.
- [86] G. Bjontegaard, "Calculation of average psnr differences between rd-curves," *VCEG-M33*, 2001.
- [87] M. Heusel, H. Ramsauer, T. Unterthiner, B. Nessler, and S. Hochreiter, "Gans trained by a two time-scale update rule converge to a local nash equilibrium," *NIPS*, 2017.
- [88] Z. Liu, X. Qi, and P. H. Torr, "Global texture enhancement for fake face detection in the wild," in *CVPR*, 2020.
- [89] P. Arbelaez, M.-P. M. Maire, C. Fowlkes, and J. Malik, "Contour detection and hierarchical image segmentation," *TPAMI*, 2010.
- [90] Z. Wang, E. P. Simoncelli, and A. C. Bovik, "Multiscale structural similarity for image quality assessment," in *ACSSC*, 2003.